

# From Binary to Semantic: Utilizing Large-Scale Binary Occupancy Data for 3D Semantic Occupancy Prediction

Chihiro Noguchi\* Takaki Yamamoto\*  
InfoTech, Toyota Motor Corporation

{chihiro.noguchi\_aa, takaki.yamamoto}@mail.toyota.co.jp

## Abstract

Accurate perception of the surrounding environment is essential for safe autonomous driving. 3D occupancy prediction, which estimates detailed 3D structures of roads, buildings, and other objects, is particularly important for vision-centric autonomous driving systems that do not rely on LiDAR sensors. However, in 3D semantic occupancy prediction—where each voxel is assigned a semantic label—annotated LiDAR point clouds are required, making data acquisition costly. In contrast, large-scale binary occupancy data, which only indicate occupied or free space without semantic labels, can be collected at a lower cost. Despite their availability, the potential of leveraging such data remains unexplored. In this study, we investigate the utilization of large-scale binary occupancy data from two perspectives: (1) pre-training and (2) learning-based auto-labeling. We propose a novel binary occupancy-based framework that decomposes the prediction process into binary and semantic occupancy modules, enabling effective use of binary occupancy data. Our experimental results demonstrate that the proposed framework outperforms existing methods in both pre-training and auto-labeling tasks, highlighting its effectiveness in enhancing 3D semantic occupancy prediction. The code will be available at <https://github.com/ToyotaInfoTech/b2s-occupancy>

## 1. Introduction

A comprehensive understanding of the surrounding 3D scene is crucial for modern autonomous driving systems. While LiDAR sensors provide an effective solution for this purpose [1–4], their high cost remains a significant drawback. In contrast, vision-based methods have gained attention due to their affordability and recent technological advancements [5–9]. This paper focuses on vision-based semantic occupancy prediction, which seeks to estimate both

\*Equal Contribution.

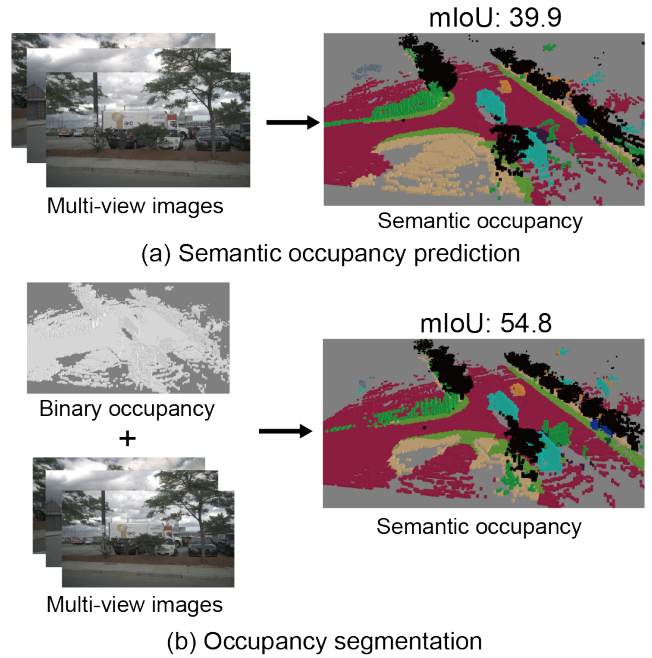


Figure 1. Compared to (a) semantic occupancy prediction, (b) occupancy segmentation utilizes binary occupancy as an additional input along with multi-view images, leading to higher performance.

the occupancy state and the semantic labels of the surrounding 3D voxels relative to the ego-vehicle.

From a practical perspective, semantic occupancy prediction faces a significant challenge due to high annotation costs [10–12]. Creating ground truth (GT) data for semantic occupancy prediction typically requires attaching semantic labels to 3D LiDAR points—a process that is both labor-intensive and costly, as it involves detailed and precise manual annotation. However, if only binary occupancy information is needed (i.e., distinguishing between occupied and free space without semantic class labels), annotation costs can be substantially reduced. This is because semantic labels and fine-grained LiDAR annotation become

unnecessary. For static scenes, binary occupancy data can be efficiently generated by aggregating LiDAR points over time, eliminating the need for point-wise semantic annotation. For dynamic objects, required data—such as 3D bounding boxes—can often be automatically created using auto-labeling systems for 3D object tracking and bounding box annotation [13–15], which are commonly available in the development environments of end-to-end autonomous driving models [16–19]. Although binary occupancy data can be collected at scale with relatively low effort, there has been limited research on how to effectively leverage them for semantic occupancy prediction.

This study investigates how large-scale binary occupancy data can improve semantic occupancy prediction. As illustrated in Fig. 1, our core idea is that if the binary occupancy is known (Fig. 1(b)), the task is reduced to simply segmenting the occupied voxels. This is significantly simpler than the original task of simultaneously learning 3D geometry and semantics (Fig. 1(a)), and we expect it to lead to better performance. Our empirical results on the Occ3D dataset confirm this, showing that using ground truth (GT) binary occupancy data boosts the mean Intersection over Union (mIoU) from 39.9 to 54.8. However, because GT data is not available during online prediction, we propose two frameworks to approximate this process using large-scale binary occupancy data.

The first framework is a pre-training approach. We leverage large-scale binary occupancy data to improve the model’s ability to predict geometric structures, thereby bringing the binary prediction performance closer to the GT level. Our experiments show that this pre-training is effective for the downstream task of semantic occupancy prediction. We also introduce a simple yet effective architecture optimized for this binary pre-training scheme.

Our second framework involves learning-based auto-labeling with binary occupancy data, a crucial technique for creating large-scale datasets where manual annotation is cost-prohibitive. In this offboard context, which has no causality constraints and minimal inference speed restrictions, binary occupancy data can be used as an input. Our results show this scheme achieves prediction performance superior to existing online methods, including multi-modal approaches, enabling it to create more accurate pseudo-labels for auto-labeling systems. To our knowledge, this is the first study to introduce an offboard semantic occupancy prediction model.

Our contributions are summarized as follows.

- We propose a simple yet effective model architecture that utilizes large-scale binary occupancy data to enhance semantic occupancy prediction.
- We experimentally demonstrate that pre-training the proposed model with binary occupancy data outperforms prevalent pre-training methods.
- We further show that the proposed model performs effectively in an offboard setting. To the best of our knowledge, this study is the first to introduce an offboard semantic occupancy prediction model.

## 2. Related Work

**Vision-based 3D perception.** Bird’s-Eye-View (BEV) representation is a fundamental technology for vision-based 3D perception [5]. Two primary approaches are commonly used to obtain a BEV representation from image features. The first approach, Lift-Splat-Shoot (LSS [20]), leverages depth distribution to project pixel-level image features into BEV space using camera calibration parameters. The second approach employs deformable attention modules, enabling BEV queries, defined in BEV space, to interact effectively with the corresponding image features [5].

**3D semantic occupancy prediction.** The goal is to assign semantic labels to each voxel in 3D space. A naive solution computes feature vectors for all voxels, but this is memory-intensive. To improve efficiency, many works explore alternative scene representations. Some use 2D planes—e.g., BEVFormer [5] (BEV) and TPVFormer [7] (tri-perspective views). Others adopt coarse-to-fine strategies [21–23] to avoid full 3D grids. COTR [24] proposes a compact 3D encoding. Sparse methods also gain traction, focusing on eliminating empty space [25–27]. OSP [28] and OPUS [29] represent scenes as point sets with refinement, while GaussianFormer [30] uses 3D Gaussians for efficient, flexible encoding. On the architectural side, OccFormer [31] introduces a dual-path transformer inspired by Mask2Former [32], and FB-OCC [33] combines LSS and BEV-based views. VoxFormer [34], most similar to our approach, also follows a two-stage design but focuses on binary occupancy data rather than semantic granularity.

**Occupancy pre-training.** Pre-training is an important strategy in 3D recognition tasks. In the context of autonomous driving, it is common to consider problem settings where LiDAR points or high-precision 3D bounding boxes are available, and pre-training using these data is widely explored [35–39]. Occupancy-based pre-training methods have also been proposed, with BEV segmentation [40] and planning [41] as downstream tasks. Additionally, UniScene [42] suggests a fine-tuning approach using a simple head exchange, although validation using large-scale occupancy data has not been conducted. This paper proposes an approach specifically focused on semantic occupancy prediction with large-scale occupancy pre-training.

**Multi-modal 3D semantic occupancy prediction.** While camera images provide rich semantic information, they lack precise geometric details. Consequently, leveraging the complementary strengths of LiDAR has become a widely adopted approach for enhancing 3D perception. Although this strategy has been extensively explored in the context of

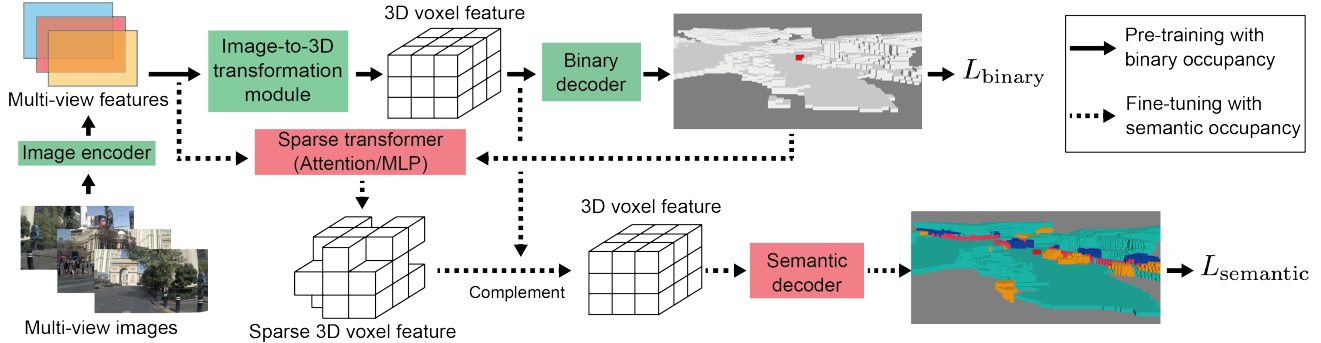


Figure 2. Overview of the model architecture. Multi-view features extracted from an image encoder are processed through an image-3D transformation module to obtain a 3D voxel feature representation. Pre-training is performed up to the binary decoder (depicted with solid lines) using  $L_{\text{binary}}$ , while fine-tuning is applied to the entire model with both  $L_{\text{binary}}$  and  $L_{\text{semantic}}$ . For learning-based auto-labeling, GT binary occupancy is used in place of the binary decoder to identify occupied regions. Red voxels at the center of occupancy images represent the ego car.

3D object detection [43–47], it is also highly effective for semantic occupancy prediction. M-CONet [10] employs a coarse-to-fine strategy to enhance computational efficiency, while Co-Occ [10] introduces implicit volume rendering regularization to bridge the gap between LiDAR and image data. In contrast to these approaches, our proposed method utilizes binary occupancy data instead of LiDAR point clouds, offering a stronger predictive performance.

**Learning-based auto-labeling.** Auto-labeling is a crucial strategy for creating large-scale GT data [16, 17] in autonomous driving systems. A common practice involves using offboard models, which are not subject to causality constraints and have minimal restrictions on inference speed. In the context of 3D object detection [13–15], offboard models have been proposed and have demonstrated significantly superior performance compared to online models. However, to the best of our knowledge, no prior work has explored an offboard approach for semantic occupancy prediction. In this study, we propose a novel method that utilizes binary occupancy data in an offboard setting.

### 3. Proposed Approach

This section is structured as follows. First, the problem setting of this study is described in Sec. 3.1. Next, an overview of the proposed model is provided in Sec. 3.2. Then, the utilization of the proposed model for binary occupancy pre-training (Sec. 3.3) and learning-based auto-labeling (Sec. 4.2) is explained.

#### 3.1. Problem Setting

Our objective is to predict the semantic occupancy surrounding the ego-vehicle using  $N$  surround-view RGB images with given camera poses and intrinsic parameters. The semantic occupancy of a scene  $i$  is represented by a 3D grid  $Y_i^s \in \{c_0, c_1, \dots, c_K\}^{H \times W \times Z}$ , which is defined in

the ego-coordinate system. Each voxel within this grid is assigned either a “free” label (denoted as  $c_0$ ) or a semantic class label from the set  $\{c_1, \dots, c_K\}$ . In contrast, the binary occupancy  $Y_i^b$  consists of “free” and “occupied” voxels, formally expressed as  $Y_i^b \in \{0, 1\}^{H \times W \times Z}$ .

In this study, we consider a situation where the available GT data for binary occupancy is significantly more abundant than that for semantic occupancy. This situation is commonly encountered in practical applications, as the generation of GT binary occupancy data does not necessitate semantic segmentation of LiDAR points.

#### 3.2. Model Overview

Figure 2 illustrates the overview of the proposed method. We decompose the semantic occupancy prediction task into two subtasks: 1) binary occupancy prediction and 2) semantic occupancy prediction using the predicted binary occupancy. Given that binary occupancy data are available in substantially larger quantities than semantic occupancy data, we can leverage this large-scale dataset to improve the binary occupancy prediction task. Our strategy employs such precise binary occupancy predictions as input for the subsequent semantic occupancy prediction module which is specifically designed to enhance the effectiveness of the binary occupancy data.

As illustrated in Fig. 2, multi-view image features are first extracted using an image encoder. These features are then transformed into a 3D voxel feature representation, denoted as  $B \in \mathbb{R}^{H^c \times W^c \times Z^c \times C}$ , via an image-to-3D transformation module (explained in detail later). The model subsequently employs a binary decoder using the 3D voxel feature as input to identify occupied regions. Here,  $H^c$ ,  $W^c$ , and  $Z^c$  represent the spatial dimension of the 3D representation, and  $C$  denotes the feature dimension. More specifically,  $B$  is upsampled to  $B' \in \mathbb{R}^{H^b \times W^b \times Z^b \times C'}$

and then used to predict the binary state of each voxel in  $B'$ . This process yields a set of feature vectors, denoted as  $\mathcal{B} = \{b_i\}_{i=1}^M$ , where  $M$  represents the number of occupied voxels predicted in  $B'$ . Notably, we adopt a 3D compact representation [24] for  $B$ , as the BEV representation lacks the  $Z$  dimension, making it unsuitable for identifying feature vectors corresponding to occupied voxels and effectively incorporating them into subsequent modules. Please refer to Appendix A for more details.

Following this step, a transformer decoder, referred to as sparse transformer, is applied to  $\mathcal{B}$  to refine its semantic representation. Consistent with [5], the sparse transformer composes deformable self/cross-attention and MLP. Since cross-attention and MLP computations are defined for each element of  $\mathcal{B}$ , the original transformer decoder [5] can be directly applied to  $\mathcal{B}$ . However, deformable self-attention cannot be directly utilized for sparse representations such as  $\mathcal{B}$ . Therefore, we instead apply deformable cross-attention [48], where each element of  $\mathcal{B}$  serves as the value, while the dense representation  $B'$  is utilized as the query and key. Finally, the enhanced  $\mathcal{B}$  is concatenated to the dense representation  $B'$  and upsampled to  $B'' \in \mathbb{R}^{H \times W \times Z \times C''}$  to predict semantic occupancy.

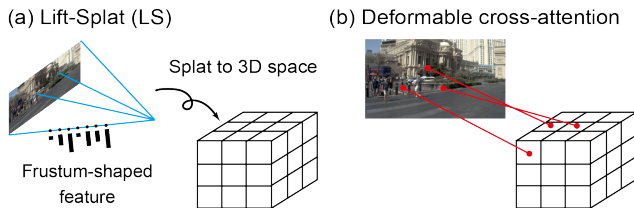


Figure 3. Schematic of Image-to-3D transformation modules. (a) Lift-Splat (LS) and (b) deformable cross-attention modules. The voxel grids represent the 3D voxel representation.

Most vision-based 3D perception methods rely on one or both of two image-to-3D transformation modules: Lift-Splat (LS) [20] and deformable cross-attention [48] (Fig. 3). In this study, we integrate the proposed pre-training module with both transformation mechanisms to ensure broad applicability. BEVFormer [5] employs deformable cross-attention, along with deformable self-attention and MLP layers. We refer to this configuration as the BEVFormer-based method, while models using the Lift-Splat mechanism are referred to as the LS-based method.

### 3.3. Binary Occupancy Pre-training

To effectively utilize large-scale binary occupancy data, we adopt a two-stage training strategy. In the first stage, training is conducted up to the binary decoder using only binary occupancy data. In the second stage, we fine-tune the entire model with both binary and semantic occupancy data. Our model architecture where the binary decoder is placed be-

fore the semantic prediction module has two key advantages in training. First, it enables efficient pre-training without negatively impacting the subsequent modules responsible for semantic occupancy prediction. Second, during the second stage of training, the same binary occupancy data utilized in pre-training can be leveraged to preserve the performance of the binary decoder. For the first stage, we employ a binary cross-entropy loss  $L_{\text{binary}}$  to optimize the binary occupancy prediction using  $B'$ . In the second stage, a focal loss  $L_{\text{semantic}}$  is utilized for semantic occupancy prediction with  $B''$ , in conjunction with  $L_{\text{binary}}$ .

There may be other strategies which aim to utilize large-scale binary occupancy data. For instance, by separating the classification heads for binary and semantic occupancy prediction, binary occupancy data could be directly employed in both pre-training and fine-tuning. However, our experimental results indicate that this approach is suboptimal (see Sec. 4.1 for further details).

### 3.4. Learning-based Auto-labeling

Auto-labeling GT of 3D semantic occupancy is critical in practice, as it enables the preparation of large-scale datasets that exceed the feasibility of manual annotation. Unlike semantic occupancy prediction in self-driving application, where online prediction is required, auto-labeling does not impose such constraints. In the context of 3D object detection, multi-modal models—commonly integrating image and LiDAR inputs—are frequently utilized as auto-labeling machines. In contrast, while several studies have explored multi-modal approaches for semantic occupancy prediction, existing research has primarily focused on online settings. For the specific purpose of auto-labeling of semantic occupancy prediction, an offboard setting must be considered to maximize the prediction performance. Since causality constraints do not apply in this context, binary occupancy data can serve as an alternative to LiDAR sweeps. Given that binary occupancy data offers denser geometric details, particularly at greater distances from the ego-vehicle, it is anticipated to be more suitable for auto-labeling tasks.

The proposed architecture for the auto-labeling setting is fundamentally the same as the online model described in Sec. 3.3. The primary distinction lies in the use of GT binary occupancy as input. Unlike the online model, the offboard model does not predict binary occupancy; instead, it leverages GT binary occupancy to identify occupied regions. The corresponding feature vectors for these occupied regions are then fed into the subsequent sparse transformer, similar to the online model. For training, only the focal loss  $L_{\text{semantic}}$  is employed.

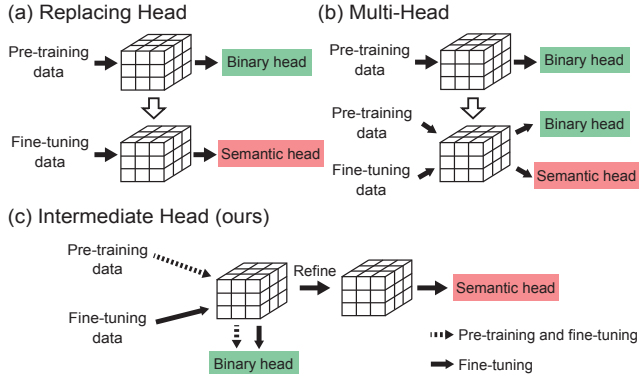


Figure 4. Schematic of baseline strategies. The voxel grids represent the 3D voxel representation.

## 4. Experiments

### 4.1. Binary Occupancy Pre-training

In this section, we experimentally validate the effectiveness of the proposed binary occupancy pre-training. To assess its impact, we evaluate the performance of semantic occupancy prediction using the pretrained model as the initial weights.

**Dataset.** We leveraged two occupancy datasets: OpenScene [49–51] and Occ3D [12]. OpenScene is the large-scale occupancy dataset generated from nuPlan [16, 17]. We randomly selected 8000 and 150 scenes for the training and validation datasets, respectively. Occ3D is an occupancy dataset derived from nuScenes [52], comprising 700 training scenes and 150 validation scenes. Both datasets provide GT with a volume size of  $200 \times 200 \times 16$ .

**Implementation Details.** The AdamW optimizer was utilized with a learning rate  $2 \times 10^{-4}$  and a weight decay of  $1 \times 10^{-2}$ , and the same augmentation strategy as BEVDet was applied [53]. Both the pre-training and fine-tuning procedures in this study were conducted over 24 epochs using a batch size of 8. For BEVFormer-based models, an image resolution of  $450 \times 800$  was utilized. To ensure a fair comparison, three dense transformer layers were applied in the original BEVFormer baselines, whereas the proposed method incorporated two dense transformer layers alongside one sparse transformer layer. For LS-based models, an image resolution of  $256 \times 704$  was utilized. The proposed method integrates one sparse transformer layer following the LS module, while the LS baselines utilize one dense transformer layer to maintain comparability. Further hyperparameter details can be found in Appendix A.

**Baselines.** During pre-training, all model parameters are updated in the baseline models. For fine-tuning, two baseline approaches are considered, as illustrated in Fig. 4. The first, *Replacing Head*, replaces the binary occupancy head with a semantic occupancy head, using only semantic occupancy data (corresponding to UniScene [42]). The second,

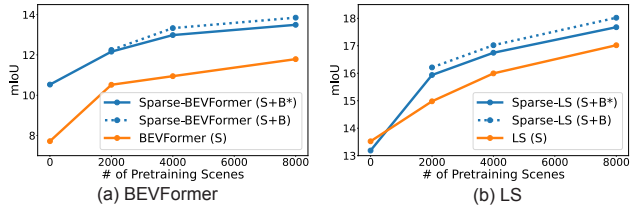


Figure 5. Performance comparison of (a) BEVFormer-based and (b) LS-based methods on OpenScene.

*Multi-Head*, adds a new semantic occupancy head while retaining the binary occupancy head, preserving some of the pre-trained binary occupancy capabilities. In comparison, our method, *Intermediate Head*, places the binary occupancy head in intermediate stages of the process. It offers two optimization options for binary occupancy loss: (1) training exclusively on binary occupancy data derived from the semantic occupancy labels (denoted as  $B^*$  in Table 1), and (2) incorporating both pre-training binary occupancy data and binary occupancy data from the semantic labels (denoted as  $B$ ). For the second option, a random batch of pre-training samples is selected to train the model up to the binary decoder.

#### 4.1.1. Comparison with Baselines

Table 1 presents the quantitative comparison with the baseline methods. The proposed fine-tuning strategy, *Intermediate Head*, achieved the best overall performance. Among the methods, the *Replacing Head* approach is the most straightforward but yielded suboptimal results. While the *Multi-Head* strategy also incorporates binary occupancy data during fine-tuning—similar to the *Intermediate Head*—it was outperformed by both other methods. Additionally, we found that the *Intermediate Head* strategy further benefits from utilizing the binary occupancy data used during pre-training, which led to even greater performance improvements (denoted as  $S+B$ ). We attribute this to the mitigation of performance degradation in binary occupancy prediction during fine-tuning under this setup, as further detailed in Appendix C. While the BEVFormer-based and LS-based methods exhibit some quantitative differences, the general trends observed across all strategies are consistent.

Figure 5 demonstrates that increasing the number of pre-training scenes consistently enhances model performance. As shown in Table 1, the proposed method outperforms the corresponding baselines for both BEVFormer- and LS-based models. For LS-based methods, the baseline and the proposed approach perform similarly when pre-training is absent; however, with more pre-training scenes, the proposed method achieves superior performance. This result highlights that our proposed architecture is particularly well-suited for leveraging pre-training strategies. Given that the evaluation accuracy in Fig. 5 has not yet saturated, even

Method	Pre-training Data	Fine-tuning Strategy	Fine-tuning Data	IoU	mIoU	Vehicle	C. Zone Sign	Bicycle	Generic Obj.	Pedestrian	Traffic Cone	Barrier	Background
BEVFormer	B	Replacing Head	S	39.03	12.77	29.90	0.00	0.00	17.17	13.40	2.35	1.32	38.01
BEVFormer	B	Multi-Head	S+B*	38.91	11.75	28.67	0.00	0.00	16.16	11.34	0.00	0.00	37.83
Sparse-BEVFormer (Ours)	B	Intermediate Head	S+B*	40.09	15.12	31.13	0.00	6.27	18.27	15.63	<b>3.72</b>	<b>6.83</b>	39.09
Sparse-BEVFormer (Ours)	B	Intermediate Head	S+B	<b>41.03</b>	<b>15.25</b>	<b>31.41</b>	0.00	<b>6.63</b>	<b>18.93</b>	<b>16.07</b>	3.48	5.45	<b>40.07</b>
LS	B	Replacing Head	S	43.08	18.35	36.35	0.01	<b>8.66</b>	21.73	19.46	<b>10.22</b>	8.27	42.07
LS	B	Multi-Head	S+B*	43.12	16.00	36.02	0.00	1.04	20.74	18.74	7.5	1.95	42.03
Sparse-LS (Ours)	B	Intermediate Head	S+B*	43.06	18.82	36.29	0.00	8.15	22.11	19.30	10.11	12.50	42.07
Sparse-LS (Ours)	B	Intermediate Head	S+B	<b>43.92</b>	<b>19.20</b>	<b>36.88</b>	<b>0.23</b>	8.00	<b>22.92</b>	<b>19.49</b>	10.20	<b>12.94</b>	<b>42.94</b>

Table 1. Quantitative comparison with baseline methods on OpenScene dataset. B and S represent binary occupancy data and semantic occupancy data, respectively. B\* denotes binary occupancy data derived only from the semantic occupancy data used in the fine-tuning. 8,000 scenes from OpenScene were used for binary occupancy pre-training, while 500 scenes were utilized for semantic occupancy fine-tuning. All models were implemented based on COTR [24] for these experiments.

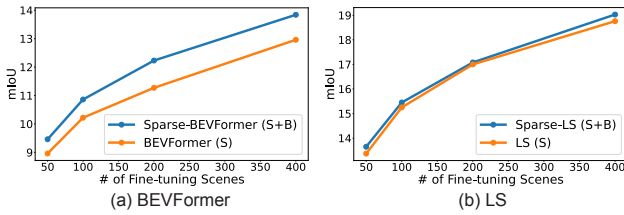


Figure 6. Performance comparison of (a) BEVFormer-based and (b) LS-based methods on nuScenes.

with 8,000 scenes, it is anticipated that performance will continue to improve with additional pre-training data. For the experiments shown in Fig. 5, 250 scenes were used for fine-tuning; additional results using 500 and 1000 fine-tuning scenes are provided in the Appendix B.

#### 4.1.2. Comparison on nuScenes

Figure 6 presents the results of experiments conducted on nuScenes. Unlike the OpenScene dataset, nuScenes does not contain a sufficient amount of training data to replicate the experimental conditions described in Sec. 4.1.1. Therefore, the objective of this section is to confirm the consistency of the obtained results with those reported in Sec. 4.1.1. Specifically, we fixed the number of pre-training scenes at 700 and varied the number of fine-tuning scenes. The proposed method demonstrated superior performance in BEVFormer-based scenarios, while achieving competitive performance in LS-based scenarios. These results are consistent with those in Sec. 4.1.1 when comparing experiments with a similar number of pre-training scenes. More specifically, the crossover point between the Sparse-LS and LS results in Fig. 5(b) corresponds to experiments conducted with approximately 500 pre-training scenes and 250 fine-tuning scenes. This experimental condition is comparable to that of Fig. 6(b). Therefore, as the number of pre-training scenes increases, the superiority of the proposed method is expected to become more pronounced.

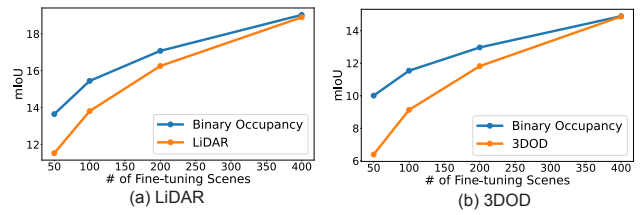


Figure 7. Comparison with (a) LiDAR and (b) 3D object detection (3DOD) pre-training methods.

#### 4.1.3. Comparison with Other Pre-training Methods

We compared the proposed binary occupancy pre-training approach with prevalent pre-training methods. Many semantic occupancy prediction methods utilize initial weights pre-trained on 3D object detection using the nuScenes dataset, as provided in [54]. Additionally, pre-training using a depth loss based on LiDAR is widely adopted, as it does not require manual annotation. For this comparison, we pre-trained on 700 scenes from nuScenes and varied the number of scenes for fine-tuning. As Figure 7 demonstrates, our proposed binary occupancy pre-training outperforms existing methods, especially when the amount of fine-tuning data is small. Although the performance gap diminishes as the number of fine-tuning scenes approaches that of the pre-training scenes, this is a general tendency in deep learning model training [55, 56]. Since the pre-training in [54] was conducted with an image resolution of  $900 \times 1600$  and a ResNet101 backbone, the pre-training and fine-tuning in Fig. 7(b) were performed under the same conditions using the BEVFormer-based model to ensure a fair comparison.

#### 4.1.4. Qualitative Evaluation

Figure 8 presents a qualitative comparison across different numbers of pre-training scenes: 0, 2000, and 8000. The top row displays the outputs of the binary decoder, while the bottom row depicts the final outputs for semantic occupancy. Notably, as the number of pre-training scenes in-

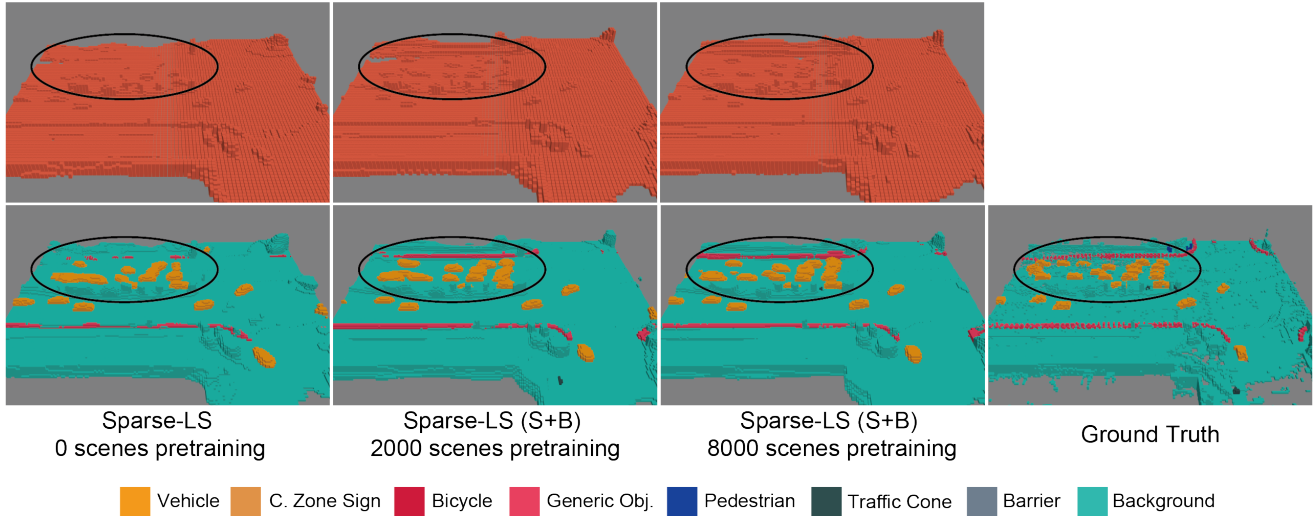


Figure 8. Qualitative comparison across different numbers of pre-training scenes: 0, 2000, and 8000. The top row presents the outputs of the binary occupancy modules, while the bottom row shows the results of semantic occupancy prediction.

creases, the refinement of detailed structures becomes more pronounced. Additionally, the detailed structures in the outputs of the binary decoder also exhibit refinement. This observation suggests that the enhancement of geometric structures learned by the binary decoder contributes to the improved geometric accuracy of semantic occupancy.

## 4.2. Learning-based Auto-labeling

In this section, we evaluate the effectiveness of the proposed auto-labeling strategy. To the best of our knowledge, the proposed method is the first to consider an offboard setting for semantic occupancy prediction. Therefore, we compare the proposed binary occupancy-based auto-labeling method with existing online models, including multi-modal models. **Dataset.** We utilized the OpenOccupancy dataset [10] to evaluate offboard prediction performance. OpenOccupancy provides 17 semantic occupancy labels for nuScenes with a volume size of  $512 \times 512 \times 40$ . Unlike other nuScenes-based occupancy benchmarks, the OpenOccupancy benchmark includes LiDAR-based baselines, making it well-suited for the objectives of this study.

**Implementation Details.** We applied the same optimizer settings as described in Sec. 4.1. Training was conducted for 64 epochs with a batch size of 8. The LS-based method was selected here, as it is expected to achieve superior results. An image resolution of  $256 \times 704$  was utilized.

### 4.2.1. Comparison with Existing Methods

Table 2 presents a quantitative comparison with existing multi-modal methods. The results show that the proposed method achieves superior performance compared to other methods. However, its performance is lower for three classes corresponding to small objects (bicycle, motorcycle,

and traffic cone) compared to methods using both camera LiDAR inputs like M-CONet and Co-Occ. We attribute this to the larger voxel size required for occupancy representations due to computational constraints (e.g., in the OpenOccupancy dataset, 0.2 in for occupancy vs. 0.1 for typical LiDAR points), which can cause fine-grained structural details to be lost. Future work may explore the use of higher image resolutions—other methods employ an image resolution of  $900 \times 1600$ —or the integration of LiDAR inputs to address this limitation.

The method’s strong overall performance makes it well-suited for auto-labeling pipelines. Although an mIoU of 33.7 is insufficient for direct use, practical setups can leverage larger models, more extensive datasets, and test-time augmentation [61] to reach acceptable accuracy. Additional results showcasing the application of the proposed method in auto-labeling pipelines are provided in Appendix D.

## 4.3. Computational Cost

We report the computational time for the pre-training and fine-tuning stages in Table 3. The pre-training on 8,000 scenes demanded over 10 days of processing on a system equipped with four A100 GPUs. In the fine-tuning stage, the use of the S+B dataset increased the required training time in comparison to the S+B\* dataset, an increase attributable to the incorporation of the B data.

## 5. Conclusion

This study introduces a learning method and architecture for 3D semantic occupancy prediction, specifically designed to leverage cost-effective binary occupancy datasets. Our approach divides the problem into two sequential steps: bi-

Method	Modality	IoU	mIoU	Offboard	barrier	bicycle	bus	car	const. veh.	motorcycle	pedestrian	traffic cone	trailer	truck	drive. suf.	other flat	sidewalk	terrain	manmade	vegetation
MonoScene [6]	C	17.1	7.2		7.3	4.3	9.6	7.1	6.2	3.5	5.9	4.7	5.6	4.9	15.6	6.8	7.9	7.6	10.5	7.9
TPVFormer [7]	C	15.1	8.3		9.7	4.5	11.5	10.7	5.5	4.6	6.3	5.4	6.9	6.9	14.1	9.8	8.9	9.0	9.9	8.5
3DSketch [57]	C&D	25.3	11.0		12.3	5.2	10.3	12.1	7.1	4.9	5.5	6.9	8.4	7.4	21.9	15.4	13.6	12.1	12.1	21.2
AICNet [58]	C&D	23.2	10.9		11.8	4.5	12.1	12.7	6.0	3.9	6.4	6.3	8.4	7.8	24.2	13.4	13.0	11.9	11.5	20.5
LMSCNet [59]	L	26.7	11.8		12.9	5.2	12.8	12.6	6.6	4.9	6.3	6.5	8.8	7.7	24.3	12.7	16.5	14.5	14.2	22.1
JS3C-Net [4]	L	29.6	12.7		14.5	4.4	13.5	12.0	7.8	4.4	7.3	6.9	9.2	9.2	27.4	15.8	15.9	16.4	14.0	24.8
M-CONet [10]	C&L	26.5	20.5		23.3	16.1	22.2	24.6	13.3	20.1	21.2	14.4	17.0	21.3	31.8	22.0	21.8	20.5	17.7	20.4
Co-Occ [60]	C&L	30.6	21.9		26.5	<b>16.8</b>	22.3	27.0	10.1	<b>20.9</b>	20.7	<b>14.5</b>	16.4	21.6	36.9	23.5	25.5	23.7	20.5	23.5
Sparse-LS (Ours)	C&B	<b>65.4</b>	<b>33.7</b>	✓	<b>34.1</b>	10.8	<b>36.4</b>	<b>40.3</b>	<b>20.2</b>	16.2	<b>28.7</b>	12.9	<b>26.9</b>	<b>32.5</b>	<b>69.2</b>	<b>37.1</b>	<b>42.7</b>	<b>43.4</b>	<b>40.7</b>	<b>46.8</b>

Table 2. Quantitative comparison on OpenOccupancy. The C, D, L, and B denote camera, depth, LiDAR, and binary occupancy, respectively. “Offboard” indicates a model operating in an offboard setting.

Stage	Training Data	Number of Pre-training Scenes	Number of Fine-tuning Scenes	Training Time (GPU Hours)
Pre-training	B	4000	0	544
Pre-training	B	8000	0	1032
Fine-tuning	S+B*	0	250	32
Fine-tuning	S+B	8000†	250	54

Table 3. Computational cost of pre-training and fine-tuning Sparse-LS. B represents binary occupancy data and S represents semantic occupancy data. The notation B\* indicates binary occupancy data that was created exclusively from the semantic data of the fine-tuning set. 8000† indicates that 250 scenes were randomly selected from 8000 scenes for each epoch.

nary occupancy prediction and semantic prediction. The model is first pre-trained on large-scale binary GT, then fine-tuned using a combination of binary and semantic data. This pre-training and fine-tuning strategy achieves superior prediction accuracy compared to simpler alternatives like the Multi-Head and Replacing Head methods. This method also functions as a learning-based auto-labeling machine using binary occupancy ground truth (GT), outperforming LiDAR or image-based models. Its higher accuracy likely stems from the richer information in binary occupancy data, including occlusion regions missed by LiDAR, and our model’s effective use of this data.

## References

- [1] Yin Zhou and Oncel Tuzel. Voxelnet: End-to-end learning for point cloud based 3d object detection. In *CVPR*, pages 4490–4499, 2018. 1
- [2] Alex H. Lang, Sourabh Vora, Holger Caesar, Lubing Zhou, Jiong Yang, and Oscar Beijbom. PointPillars: Fast Encoders for Object Detection From Point Clouds. In *CVPR*, pages 12697–12705, 2019.
- [3] Tianwei Yin, Xingyi Zhou, and Philipp Krahenbuhl. Center-Based 3D Object Detection and Tracking. In *CVPR*, pages 11784–11793, 2021.
- [4] Xu Yan, Jiantao Gao, Jie Li, Ruimao Zhang, Zhen Li, Rui Huang, and Shuguang Cui. Sparse Single Sweep LiDAR Point Cloud Segmentation via Learning Contextual Shape Priors from Scene Completion. *AAAI*, pages 3101–3109, 2021. 1, 8
- [5] Zhiqi Li, Wenhai Wang, Hongyang Li, Enze Xie, Chonghao Sima, Tong Lu, Qiao Yu, and Jifeng Dai. Bevformer: Learning bird’s-eye-view representation from lidar-camera via spatiotemporal transformers. In *ECCV*, 2022. 1, 2, 4
- [6] Anh-Quan Cao and Raoul De Charette. Monoscene: Monocular 3d semantic scene completion. In *CVPR*, pages 3991–4001, 2022. 8
- [7] Yuanhui Huang, Wenzhao Zheng, Yunpeng Zhang, Jie Zhou, and Jiwen Lu. Tri-perspective view for vision-based 3d semantic occupancy prediction. In *CVPR*, pages 9223–9232, 2023. 2, 8
- [8] Yihan Hu, Jiazhi Yang, Li Chen, Keyu Li, Chonghao Sima, Xizhou Zhu, Siqi Chai, Senyao Du, Tianwei Lin, Wenhai Wang, Lewei Lu, Xiaosong Jia, Qiang Liu, Jifeng Dai, Yu Qiao, and Hongyang Li. Planning-Oriented Autonomous Driving. In *CVPR*, pages 17853–17862, 2023.
- [9] Bo Jiang, Shaoyu Chen, Qing Xu, Bencheng Liao, Jiajie Chen, Helong Zhou, Qian Zhang, Wenyu Liu, Chang Huang, and Xinggang Wang. VAD: Vectorized Scene Representation for Efficient Autonomous Driving. In *ICCV*, pages 8340–8350, 2023. 1
- [10] Xiaofeng Wang, Zheng Zhu, Wenbo Xu, Yunpeng Zhang, Yi Wei, Xu Chi, Yun Ye, Dalong Du, Jiwen Lu, and Xinggang Wang. OpenOccupancy: A Large Scale Benchmark for Surrounding Semantic Occupancy Perception. In *ICCV*, pages 17850–17859, 2023. 1, 3, 7, 8
- [11] Yi Wei, Linqing Zhao, Wenzhao Zheng, Zheng Zhu, Jie Zhou, and Jiwen Lu. SurroundOcc: Multi-camera 3D Occupancy Prediction for Autonomous Driving. In *ICCV*, pages 21729–21740, 2023.
- [12] Xiaoyu Tian, Tao Jiang, Longfei Yun, Yucheng Mao, Huitong Yang, Yue Wang, Yilun Wang, and Hang Zhao. Occ3D: A Large-Scale 3D Occupancy Prediction Benchmark for Autonomous Driving. *NeurIPS*, pages 64318–64330, 2023. 1, 5
- [13] Charles R Qi, Yin Zhou, Mahyar Najibi, Pei Sun, Khoa Vo, Boyang Deng, and Dragomir Anguelov. Offboard 3d object detection from point cloud sequences. In *CVPR*, pages 6134–6144, 2021. 2, 3
- [14] Tao Ma, Xueming Yang, Hongbin Zhou, Xin Li, Botian Shi, Junjie Liu, Yuchen Yang, Zhizheng Liu, Liang He, Yu Qiao, et al. Detzero: Rethinking offboard 3d object detection with

- long-term sequential point clouds. In *ICCV*, pages 6736–6747, 2023.
- [15] Lue Fan, Yuxue Yang, Yiming Mao, Feng Wang, Yuntao Chen, Naiyan Wang, and Zhaoxiang Zhang. Once detected, never lost: Surpassing human performance in offline lidar based 3d object detection. In *ICCV*, pages 19820–19829, 2023. 2, 3
- [16] Napat Karnchanachari, Dimitris Geromichalos, Kok Seang Tan, Nanxiang Li, Christopher Eriksen, Shakiba Yaghoubi, Noushin Mehdipour, Gianmarco Bernasconi, Whye Kit Fong, Yiluan Guo, and Holger Caesar. Towards learning-based planning: The nuPlan benchmark for real-world autonomous driving. In *ICRA*, pages 629–636, 2024. 2, 3, 5
- [17] Holger Caesar, Juraj Kabzan, Kok Seang Tan, Whye Kit Fong, Eric Wolff, Alex Lang, Luke Fletcher, Oscar Beijbom, and Sammy Omari. NuPlan: A closed-loop ML-based planning benchmark for autonomous vehicles. *arXiv preprint arXiv:2106.11810*, 2022. 3, 5
- [18] Pei Sun, Henrik Kretzschmar, Xerxes Dotiwalla, Aurelien Chouard, Vijaysai Patnaik, Paul Tsui, James Guo, Yin Zhou, Yuning Chai, Benjamin Caine, et al. Scalability in perception for autonomous driving: Waymo open dataset. In *CVPR*, pages 2446–2454, 2020.
- [19] Wod vision-based end-to-end driving challenge. <https://waymo.com/open/challenges/2025/e2e-driving>, 2023. 2
- [20] Jonah Philion and Sanja Fidler. Lift, Splat, Shoot: Encoding Images from Arbitrary Camera Rigs by Implicitly Unprojecting to 3D. In *ECCV*, pages 194–210, 2020. 2, 4
- [21] Wenwen Tong, Chonghao Sima, Tai Wang, Li Chen, Silei Wu, Hanming Deng, Yi Gu, Lewei Lu, Ping Luo, Dahua Lin, et al. Scene as occupancy. In *ICCV*, pages 8406–8415, 2023. 2
- [22] Yi Wei, Linqing Zhao, Wenzhao Zheng, Zheng Zhu, Jie Zhou, and Jiwen Lu. Surroundocc: Multi-camera 3d occupancy prediction for autonomous driving. In *ICCV*, pages 21729–21740, 2023.
- [23] Yuqi Wang, Yuntao Chen, Xingyu Liao, Lue Fan, and Zhaoxiang Zhang. Panoocc: Unified occupancy representation for camera-based 3d panoptic segmentation. In *CVPR*, pages 17158–17168, 2024. 2
- [24] Qihang Ma, Xin Tan, Yanyun Qu, Lizhuang Ma, Zhizhong Zhang, and Yuan Xie. COTR: Compact Occupancy TRansformer for Vision-based 3D Occupancy Prediction. In *CVPR*, pages 19936–19945, 2024. 2, 4, 6
- [25] Yuhang Lu, Xinge Zhu, Tai Wang, and Yuexin Ma. Occtreeocc: Efficient and multi-granularity occupancy prediction using octree queries. *arXiv preprint arXiv:2312.03774*, 2024. 2
- [26] Haisong Liu, Yang Chen, Haiguang Wang, Zetong Yang, Tianyu Li, Jia Zeng, Li Chen, Hongyang Li, and Limin Wang. Fully sparse 3d occupancy prediction. In *ECCV*, pages 54–71, 2024.
- [27] Pin Tang, Zhongdao Wang, Guoqing Wang, Jilai Zheng, Xianguan Ren, Bailan Feng, and Chao Ma. Sparseocc: Rethinking sparse latent representation for vision-based semantic occupancy prediction. In *CVPR*, pages 15035–15044, 2024. 2
- [28] Yiang Shi, Tianheng Cheng, Qian Zhang, Wenyu Liu, and Xinggang Wang. Occupancy as set of points. In *ECCV*, pages 72–87, 2024. 2
- [29] Jiabao Wang, Zhaojiang Liu, Qiang Meng, Liujiang Yan, Ke Wang, Jie Yang, Wei Liu, Qibin Hou, and Ming-Ming Cheng. Opus: occupancy prediction using a sparse set. In *NeurIPS*, 2024. 2
- [30] Yuanhui Huang, Wenzhao Zheng, Yunpeng Zhang, Jie Zhou, and Jiwen Lu. Gaussianformer: Scene as gaussians for vision-based 3d semantic occupancy prediction. In *ECCV*, pages 376–393, 2024. 2
- [31] Yunpeng Zhang, Zheng Zhu, and Dalong Du. Occformer: Dual-path transformer for vision-based 3d semantic occupancy prediction. In *ICCV*, pages 9433–9443, 2023. 2
- [32] Bowen Cheng, Ishan Misra, Alexander G Schwing, Alexander Kirillov, and Rohit Girdhar. Masked-attention mask transformer for universal image segmentation. In *CVPR*, pages 1290–1299, 2022. 2
- [33] Zhiqi Li, Zhiding Yu, David Austin, Mingsheng Fang, Shiyi Lan, Jan Kautz, and Jose M Alvarez. Fb-occ: 3d occupancy prediction based on forward-backward view transformation. *arXiv preprint arXiv:2307.01492*, 2023. 2
- [34] Yiming Li, Zhiding Yu, Christopher Choy, Chaowei Xiao, Jose M Alvarez, Sanja Fidler, Chen Feng, and Anima Anandkumar. Voxformer: Sparse voxel transformer for camera-based 3d semantic scene completion. In *CVPR*, pages 9087–9098, 2023. 2
- [35] Hanxue Liang, Chenhan Jiang, Dapeng Feng, Xin Chen, Hang Xu, Xiaodan Liang, Wei Zhang, Zhenguo Li, and Luc Van Gool. Exploring geometry-aware contrast and clustering harmonization for self-supervised 3d object detection. In *ICCV*, pages 3293–3302, 2021. 2
- [36] Junbo Yin, Dingfu Zhou, Liangjun Zhang, Jin Fang, Cheng-Zhong Xu, Jianbing Shen, and Wenguan Wang. Proposal-contrast: Unsupervised pre-training for lidar-based 3d object detection. In *ECCV*, pages 17–33. Springer, 2022.
- [37] Jiakang Yuan, Bo Zhang, Xiangchao Yan, Botian Shi, Tao Chen, Yikang Li, and Yu Qiao. Ad-pt: Autonomous driving pre-training with large-scale point cloud dataset. *NeurIPS*, 36:47914–47933, 2023.
- [38] Alexandre Boulch, Corentin Sautier, Björn Michele, Gilles Puy, and Renaud Marlet. Also: Automotive lidar self-supervision by occupancy estimation. In *CVPR*, pages 13455–13465, 2023.
- [39] Chen Min, Liang Xiao, Dawei Zhao, Yiming Nie, and Bin Dai. Occupancy-mae: Self-supervised pre-training large-scale lidar point clouds with masked occupancy autoencoders. *TIV*, 9(7):5150–5162, 2023. 2
- [40] Sophia Sirko-Galouchenko, Alexandre Boulch, Spyros Gidaris, Andrei Bursuc, Antonin Vobecky, Patrick Pérez, and Renaud Marlet. Occfeat: Self-supervised occupancy feature prediction for pretraining bev segmentation networks. In *CVPRW*, pages 4493–4503, 2024. 2
- [41] Chen Min, Dawei Zhao, Liang Xiao, Jian Zhao, Xinli Xu, Zheng Zhu, Lei Jin, Jianshu Li, Yulan Guo, Junliang Xing, et al. Driveworld: 4d pre-trained scene understanding via world models for autonomous driving. In *CVPR*, pages 15522–15533, 2024. 2

- [42] Chen Min, Liang Xiao, Dawei Zhao, Yiming Nie, and Bin Dai. Multi-camera unified pre-training via 3d scene reconstruction. *IEEE Robot. Autom. Lett.*, 9(4):3243–3250, 2024. 2, 5
- [43] Xiaozhi Chen, Huimin Ma, Ji Wan, Bo Li, and Tian Xia. Multi-view 3d object detection network for autonomous driving. In *CVPR*, pages 1907–1915, 2017. 3
- [44] Yingwei Li, Adams Wei Yu, Tianjian Meng, Ben Caine, Jiquan Ngiam, Daiyi Peng, Junyang Shen, Yifeng Lu, Denny Zhou, Quoc V Le, et al. Deepfusion: Lidar-camera deep fusion for multi-modal 3d object detection. In *CVPR*, pages 17182–17191, 2022.
- [45] Zehui Chen, Zhenyu Li, Shiquan Zhang, Liangji Fang, Qin-hong Jiang, and Feng Zhao. BEVDistill: Cross-modal BEV distillation for multi-view 3d object detection. In *ICLR*, 2023.
- [46] Zhijian Liu, Haotian Tang, Alexander Amini, Xinyu Yang, Huiyi Mao, Daniela L Rus, and Song Han. Bevfusion: Multi-task multi-sensor fusion with unified bird’s-eye view representation. In *ICRA*, pages 2774–2781, 2023.
- [47] Xiaotian Li, Baojie Fan, Jiandong Tian, and Huijie Fan. Gafusion: Adaptive fusing lidar and camera with multiple guidance for 3d object detection. In *CVPR*, pages 21209–21218, 2024. 3
- [48] Xizhou Zhu, Weijie Su, Lewei Lu, Bin Li, Xiaogang Wang, and Jifeng Dai. Deformable detr: Deformable transformers for end-to-end object detection. In *ICLR*, 2021. 4
- [49] Zetong Yang, Li Chen, Yanan Sun, and Hongyang Li. Visual point cloud forecasting enables scalable autonomous driving. *arXiv preprint arXiv:2312.17655*, 2023. 5
- [50] OpenScene Contributors. Openscene: The largest up-to-date 3d occupancy prediction benchmark in autonomous driving. <https://github.com/OpenDriveLab/OpenScene>, 2023.
- [51] Chonghao Sima, Wenwen Tong, Tai Wang, Li Chen, Silei Wu, Hanming Deng, Yi Gu, Lewei Lu, Ping Luo, Dahua Lin, and Hongyang Li. Scene as occupancy. 2023. 5
- [52] Holger Caesar, Varun Bankiti, Alex H Lang, Sourabh Vora, Venice Erin Liong, Qiang Xu, Anush Krishnan, Yu Pan, Giancarlo Baldan, and Oscar Beijbom. nuscenes: A multimodal dataset for autonomous driving. In *CVPR*, pages 11621–11631, 2020. 5
- [53] Junjie Huang, Guan Huang, Zheng Zhu, Yun Ye, and Dalong Du. BEVDet: High-performance Multi-camera 3D Object Detection in Bird-Eye-View. *arXiv preprint arXiv:2112.11790*, 2022. 5
- [54] Tai Wang, Xinge Zhu, Jiangmiao Pang, and Dahua Lin. Fcos3d: Fully convolutional one-stage monocular 3d object detection. In *ICCV*, pages 913–922, 2021. 6
- [55] Kaiming He, Ross Girshick, and Piotr Dollár. Rethinking imagenet pre-training. In *ICCV*, pages 4918–4927, 2019. 6
- [56] Ziquan Liu, Yi Xu, Yuanhong Xu, Qi Qian, Hao Li, Xiangyang Ji, Antoni Chan, and Rong Jin. Improved fine-tuning by better leveraging pre-training data. *NeurIPS*, 35:32568–32581, 2022. 6
- [57] Xiaokang Chen, Kwan-Yee Lin, Chen Qian, Gang Zeng, and Hongsheng Li. 3D Sketch-Aware Semantic Scene Completion via Semi-Supervised Structure Prior. In *CVPR*, pages 4192–4201, 2020. 8
- [58] Jie Li, Kai Han, Peng Wang, Yu Liu, and Xia Yuan. Anisotropic Convolutional Networks for 3D Semantic Scene Completion. In *CVPR*, pages 3351–3359, 2020. 8
- [59] Luis Roldão, Raoul de Charette, and Anne Verroust-Blondet. LMSCNet: Lightweight Multiscale 3D Semantic Completion. In *3DV*, pages 111–119, 2020. 8
- [60] Jingyi Pan, Zipeng Wang, and Lin Wang. Co-occ: Coupling explicit feature fusion with volume rendering regularization for multi-modal 3d semantic occupancy prediction. *IEEE RA-L*, 2024. 8
- [61] Nikita Moshkov, Botond Mathe, Attila Kertesz-Farkas, Reka Hollandi, and Peter Horvath. Test-time augmentation for deep learning-based cell segmentation on microscopy images. *Sci. Rep.*, 10(1):5068, 2020. 7

# From Binary to Semantic: Utilizing Large-Scale Binary Occupancy Data for 3D Semantic Occupancy Prediction

## Supplementary Material

### A. Implementation Details

#### A.1. 3D Representation

As discussed in Sec. 3.2, we employed a 3D compact representation rather than a BEV representation. The primary limitation of the BEV representation is the absence of the  $Z$  dimension, while it retains full resolution along the  $H$  and  $W$  dimensions (typically  $H = 200$  and  $W = 200$ ). To perform binary occupancy prediction from the BEV representation, the channel dimension  $C$  must be reshaped (e.g.,  $C = 512$  is typically reshaped as  $Z \times C' = 16 \times 32 = 512$ ). However, this transformation presents two challenges for our approach.

First, the reduced channel dimension  $C' = 32$  is insufficient for the subsequent sparse transformer, potentially creating a bottleneck in the model. Second, the full resolution of the 3D space (typically  $H = 200$ ,  $W = 200$ , and  $Z = 16$ ) is computationally prohibitive for real-time applications. Consequently, it is necessary to downsample the spatial resolution from  $(H, W) = (200, 200)$  to  $(H', W') = (100, 100)$ , which may introduce an additional bottleneck in the model.

To mitigate these limitations, the proposed model adopts a 3D compact representation with  $H^c = 50$ ,  $W^c = 50$ ,  $Z^c = 16$ , and  $C = 256$ , thereby addressing the aforementioned concerns. The representation is then upsampled to a resolution of  $H^b = 100$ ,  $W^b = 100$ , and  $Z^c = 16$  for binary occupancy prediction. For auto-labeling experiments, we employed higher-resolution setting with  $H^c = H^b = 256$ ,  $W^c = W^b = 256$ ,  $Z^c = Z^b = 40$ , and  $C = 64$ , as the OpenOccupancy dataset provides a larger volume size ( $H = 512$ ,  $W = 512$ ,  $Z = 40$ ), and the auto-labeling experiments consider only an offboard setting.

#### A.2. Architecture Details

For both LS-based and BEVFormer-based methods we employed a ResNet50 backbone with a FPN as the neck. The standard transformer in BEVFormer utilizes spatially dense queries and is therefore referred to as a dense transformer in the main text. In contrast, the proposed method incorporates a sparse transformer, which utilizes feature vectors corresponding to occupied regions as queries, as explained in Sec. 3.2. In both transformer architectures, we adopted the following hyperparameters: the number of attention heads is set to 8, the number of reference points for deformable attention is 4 in the self-attention module and 8 in the cross-

attention module, and the embedding dimension is 256. For further implementation details, please refer to the provided code.

### B. Evaluating Semantic Occupancy Prediction with Varying Numbers of Fine-tuning Scenes

In Section 4.1.1, we presented experimental results using 250 fine-tuning scenes. Figure 9 provides additional results with 500 and 1000 fine-tuning scenes. The proposed method consistently demonstrates a performance advantage across all fine-tuning set sizes.

### C. Evaluating Binary Occupancy Prediction During Pre-training

Figure 10 provides the IoU scores of the binary occupancy prediction module within the proposed method as a function of the number of pre-training scenes. The IoU scores are highest upon the completion of pre-training but decrease during fine-tuning, as the number of fine-tuning scenes is substantially smaller than that of pre-training scenes. However, the proposed fine-tuning strategy effectively mitigates this performance degradation by incorporating the pre-training scenes during fine-tuning.

### D. Performance Evaluation in Auto-labeling Pipelines

In Sec. 4.2, we evaluated the proposed auto-labeling model using the OpenOccupancy dataset. However, OpenOccupancy is not sufficiently large to evaluate auto-labeling pipelines. Therefore, in this section, we utilize the OpenScene dataset to generate a large-scale semantic occupancy dataset using the proposed pipeline and evaluate its effectiveness by training online methods on the generated dataset.

Table 4 presents a comparison of Sparse-LSS in an offboard setting—where GT binary occupancy is provided as input—versus an onboard setting. Consistent with the results on OpenOccupancy, the offboard model achieves significantly higher performance than its onboard counterparts.

Using the trained offboard model, we generated pseudo-labels. However, dense predictions such as semantic occupancy prediction require substantial storage capacity to save the generated labels. Ideally, storing logits for all voxels

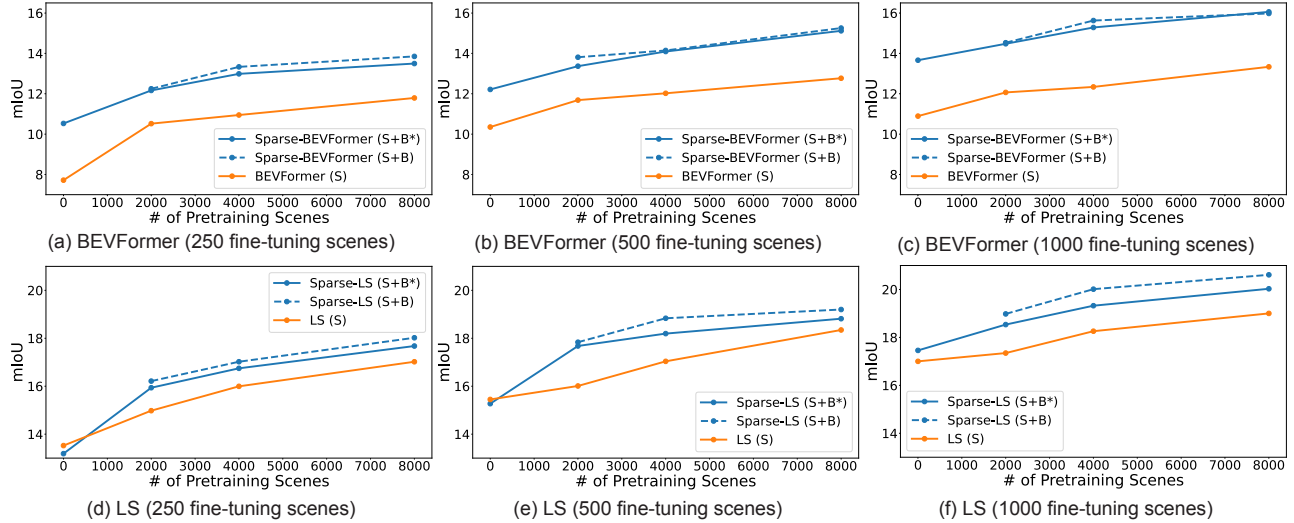


Figure 9. These figures display the mIoU scores as the number of pre-training scenes varies. The top row shows the results of BEVFormer-based models, while the bottom row presents the results of LS-based models.

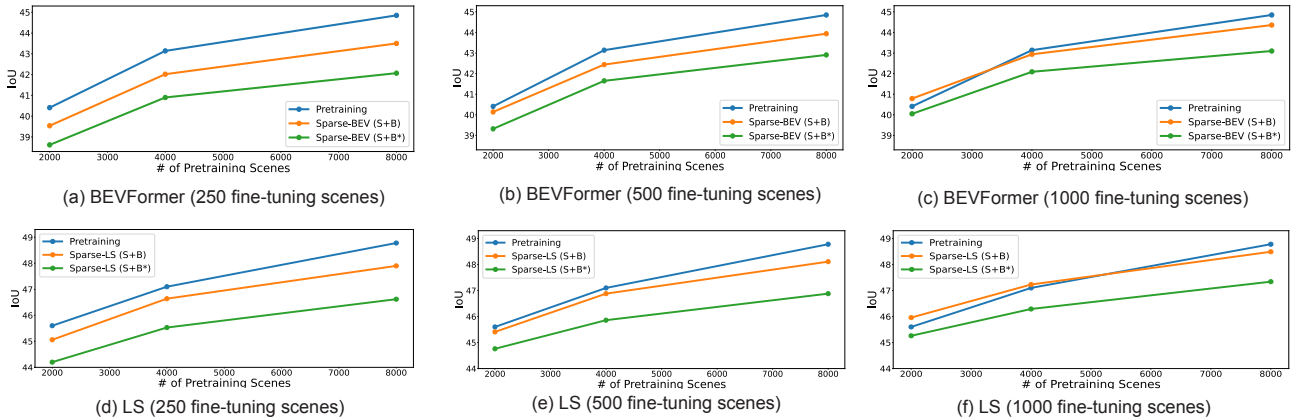


Figure 10. These figures display the IoU scores of binary occupancy prediction module with the proposed method as a function of the number of pre-training scenes.

would maximize performance, but this is impractical due to storage constraints. Therefore, in our experiments, we compared two types of pseudo-labeling approaches. The first is a storage-efficient approach, where only label indices corresponding to the highest predicted probability are stored (denoted as “Top1” in Tab. 5). The second is a balanced approach, where the top two logits are stored (denoted as “Top2” in Tab. 5).

As a baseline, we trained an LS-based model on 500 scenes with GT semantic occupancy labels. From this baseline, we progressively increased the number of scenes with pseudo-labels. As shown in Tab. 5, both IoU and mIoU improve as the number of pseudo-labeled scenes increases. Additionally, as expected, the Top2 strategy outperforms the Top1 strategy, demonstrating the benefits of retaining

more predictive information. Notably, when 7,500 pseudo-labeled scenes are used, the model’s performance becomes competitive with that of a model trained on 2,000 scenes with GT labels, highlighting the effectiveness of pseudo-labeling in reducing reliance on manually annotated data.

## E. Performance Comparison with Longer Epochs

All experiments in Sec. 4.1 were conducted with 24 epochs. We here present experimental results with an extended fine-tuning duration of 64 epochs, during which the mIoU scores fully reach the plateau. As illustrated in Figure 11, our strategy outperforms the baseline by achieving higher plateau mIoU scores.

Method	Offboard	IoU	mIoU	Vehicle	C. Zone Sign	Bicycle	Generic Object	Pedestrian	Traffic Cone	Barrier	Background
Sparse-LS		43.92	19.20	36.88	0.23	8.00	22.92	19.49	10.20	12.94	42.94
Sparse-LS	✓	<b>73.89</b>	<b>33.17</b>	62.44	6.67	10.11	33.38	37.62	23.08	19.60	72.44

Table 4. Performance comparison between offboard and onboard models on the OpenScene dataset. The onboard model was pretrained on 8000 scenes and fine-tuned on 500 scenes. The offboard model was trained on the same 500 scenes dataset.

Method	# of Scenes w/ GT	# of Scenes w/ Pseudo-labels	Pseudo-labels	IoU	mIoU
LS	500	0	-	37.70	15.45
LS	2000	0	-	41.12	18.76
LS	500	1500	Top1	37.62	17.10
LS	500	1500	Top2	44.62	17.40
LS	500	3500	Top1	38.24	17.55
LS	500	3500	Top2	<b>46.09</b>	18.11
LS	500	7500	Top1	38.72	<b>18.22</b>

Table 5. Evaluation results of the auto-labeling pipelines using the proposed offboard model. Top1 denotes the auto-labeling approach in which only label indices corresponding to the highest predicted probability are stored, whereas Top2 represents the approach where the top two logits are stored.

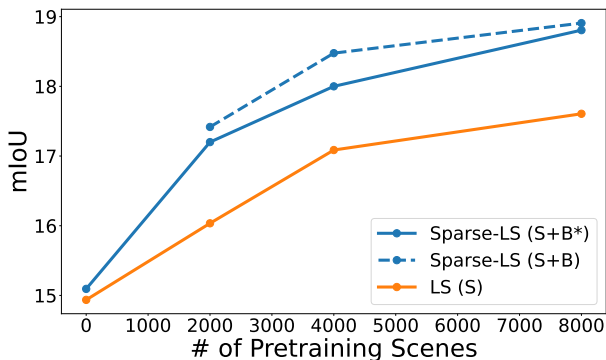


Figure 11. mIoU scores at 64 epoch as a function of the number of pre-training scenes. 250 scenes are used for the fine-tuning.

## F. Qualitative Evaluation

Figures 12-16 present representative examples of the outputs generated by the proposed method, which are omitted from Sec. 4.1.4 in the main text due to page limitations.

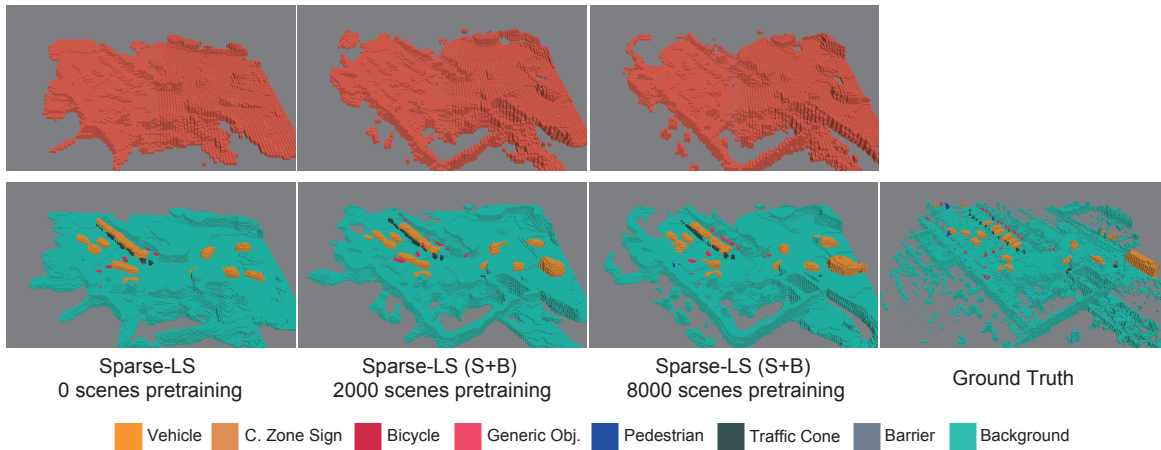


Figure 12. Qualitative comparison across different numbers of pre-training scenes: 0, 2000, and 8000. The top row presents the outputs of the binary occupancy modules, while the bottom row shows the results of semantic occupancy prediction.

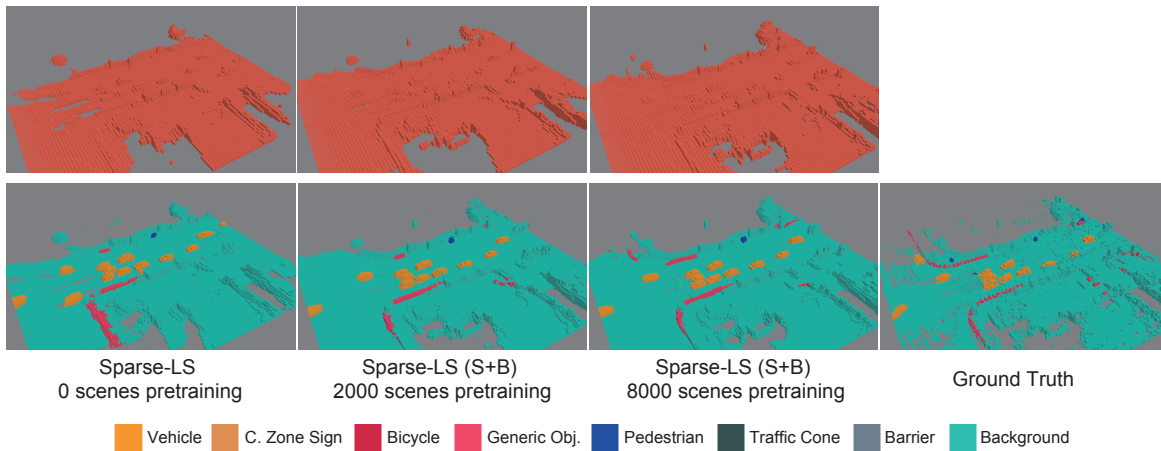


Figure 13. Refer to the caption of Figure 12 for a detailed description.

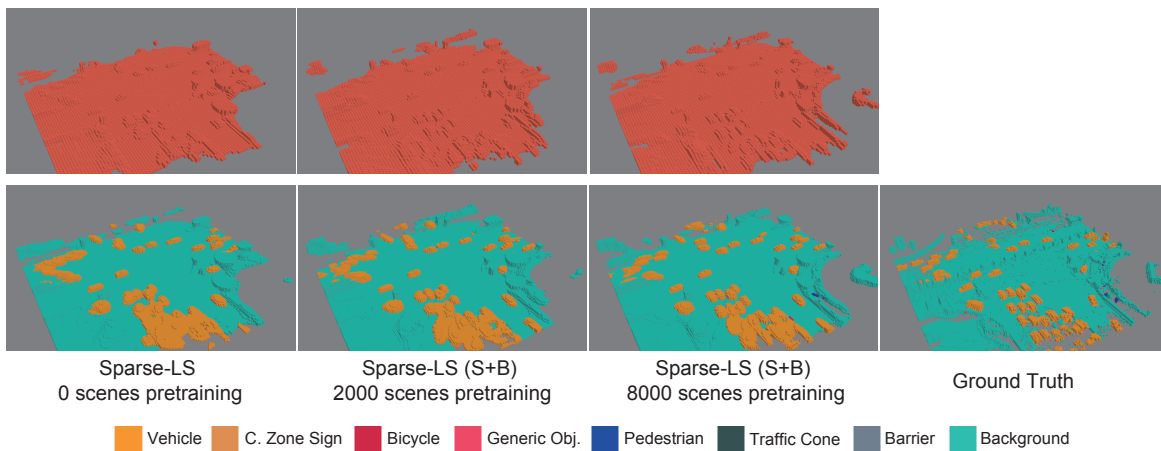


Figure 14. Refer to the caption of Figure 12 for a detailed description.

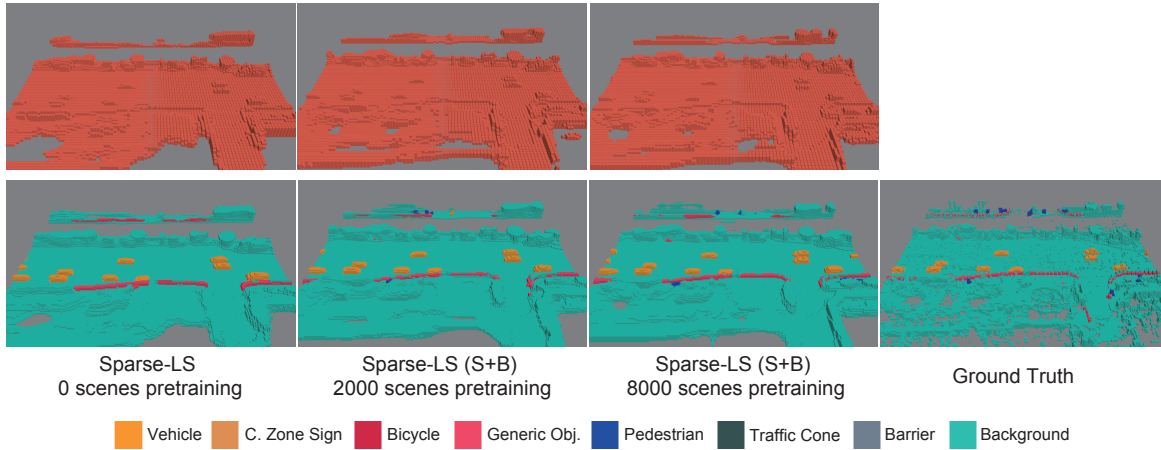


Figure 15. Refer to the caption of Figure 12 for a detailed description.

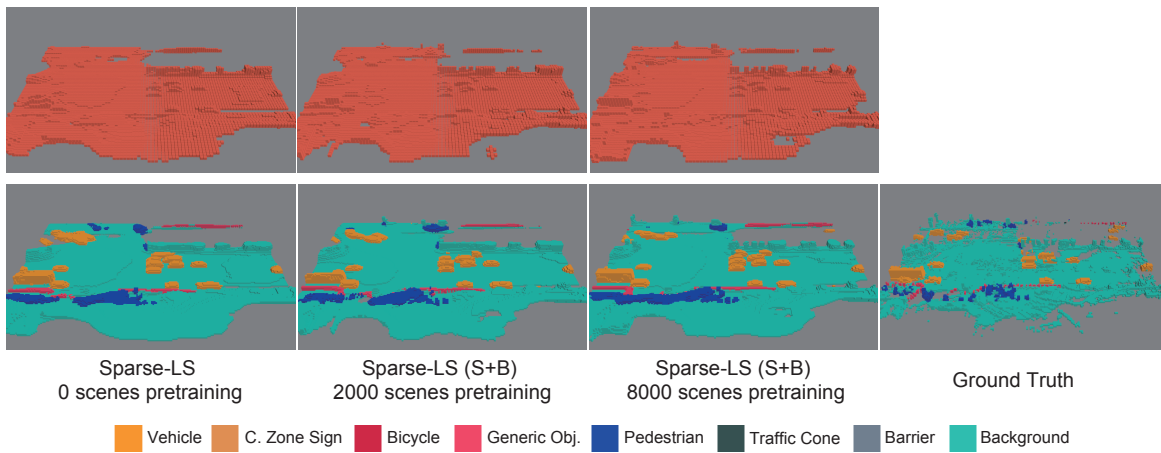


Figure 16. Refer to the caption of Figure 12 for a detailed description.